Optimizing Power Density and Efficiency of a Double-Halbach Array Permanent-Magnet Ironless Axial-Flux Motor

Kirsten P. Duffy[1]

University of Toledo, Cleveland, Ohio, 44135

NASA Glenn Research Center is investigating hybrid electric and turboelectric propulsion concepts for future aircraft to reduce fuel burn, emissions, and noise. Systems studies show that the weight and efficiency of the electric system components need to be improved for this concept to be feasible. This effort aims to identify design parameters that affect power density and efficiency for a double-Halbach array permanent-magnet ironless axial flux motor configuration. These parameters include both geometrical and higher-order parameters, including pole count, rotor speed, current density, and geometries of the magnets, windings, and air gap.

Nomenclature

B_R	=	permanent magnet remanence flux (T)
B	=	magnetic flux density (T)
d	=	conductor strand diameter (m)
f	=	frequency (Hz)
F	=	force (N)
I	=	current (A-turns)
J	=	current density (A/m^2)
k	=	wavenumber of pole pair (rad/m)
m	=	mass (kg)
n_m	=	number of magnets comprising a pole pair
p	=	number of pole pairs
P	=	power (W)
r	=	distance in radial direction (m)
T	=	torque (N-m)
V	=	volume (m^3)
x	=	distance in circumferential direction (m)
y	=	distance in axial direction (m)
z	=	distance in radial direction (m)
ϵ	=	magnet embrace
ρ	=	mass density (kg/m^3)
σ	=	conductivity (S/m)
ω_r	=	rotor angular speed (rad/s)

Subscripts:

a	=	average value
A	=	phase A
B	=	phase B
c	=	conductor or coil
C	=	phase C
e	=	eddy
g	=	gap

---

[1] Senior Research Associate, NASA Glenn Research Center, 21000 Brookpark Road, MS 49-8, Cleveland, Ohio 44139, member AIAA.

1

American Institute of Aeronautics and Astronautics

m	=	magnet
p	=	pole pair

I. Introduction

NASA Glenn Research Center is investigating hybrid electric propulsion and turboelectric propulsion for future aircraft to reduce fuel burn and emissions, and to enable technologies that will reduce aircraft noise. A study conducted by Boeing titled Subsonic Ultra Green Aircraft Research[1] showed that the use of hybrid electric propulsion significantly improved fuel burn and emissions for a 154-passenger aircraft. However, the weight and efficiency of the electric system components must be improved before hybrid electric or turboelectric propulsion is feasible. At NASA Glenn Research Center, Brown[2] performed an analysis of room temperature hybrid electric propulsion for a 150-passenger aircraft. He concluded that a motor with a total power density (motor and casing) of 4.9 kW/kg (3 HP/lb) and 97% efficiency would lead to an approximate 10% increase in aircraft weight. Much of this weight increase is due to battery weight. One goal for hybrid gas-electric propulsion is to develop electric machines with better than 96% efficiency and 13 kW/kg (8 HP/lb) power density in order to provide benefits to the aircraft. However, there are many combinations of power density and efficiency that could succeed for given aircraft configurations; for example, increasing efficiency results in lower required power density. To explore that design space, Jansen[3] estimated the combinations of total electrical system power density and efficiency required to break even in a cost-benefit analysis for turboelectric aircraft. Based on the results of that study, it was decided to investigate various motor configurations with the target of 13 kW/kg and very low loss (1%).

One of the motor designs chosen for study is an axial flux double-Halbach array permanent-magnet (PM) ironless motor, which will be described in this paper. It was chosen as a candidate motor since there will be no iron loss; the Halbach array concentrates the flux density well within the air gap, which increases torque; and there is a possibility of using compact, printed circuit board windings within the air gap. The effort described here aimed to identify design parameters that affect motor performance, including both geometrical and higher-order parameters such as pole count, rotor speed, current density, and geometries of the magnets, windings, and air gap.

The axial flux permanent magnet motor has been investigated by numerous researchers, and a thorough explanation of the many aspects of these machines is given by Gieras, Wang, and Kamper[4]. In their 2012 publication, Capponi, De Donato, and Caricchi[5] reviewed the analysis and design progress in the literature, including electromagnetic modeling. They included discussion of the 2-D, 3-D, analytical and finite element modeling. One of the difficulties in performing finite element analysis of axial flux motor is that time-consuming three-dimensional models are required. Utilizing first principles equations for the magnetic flux within the motor is one way to produce quicker results, as was done by Virtič et al. for a coreless axial flux PM motor.[6] A similar analysis is done here, but for a slotless and coreless double-Halbach PM array.

This type of analysis is a good approximation of the motor performance, but for an explanation of more thorough analysis techniques, see the following publications. Huang, Luo, Leonardi, and Lipo[7] presented the sizing equations and power densities for axial flux machines, showing performance was up to three times better than induction machines. They found that the ratio of inner to outer diameter of the rotor affects the power density more than efficiency. Mahmoudi, Rahim, and Ping[8] looked at a double-sided slotted axial flux permanent magnet motor with application to an electric vehicle drive. They used sizing equations as well as 3D finite element analysis to design a 10 kW motor the goal of better than 90% efficiency. Bumby et al.[9] investigated a slotless axial flux PM motor, using analytical models in addition to 2D and 3D finite element analysis, using two existing generators as examples.

II. Application

The target application was chosen to be the HEIST (Hybrid-Electric Integrated Systems Testbed) ground-based distributed motor-driven fan test.[10] This testbed at NASA Armstrong Flight Research Center consists of a 31-foot span wing section with 18 electric motors powered by batteries. The motors currently being used are radial-flux permanent magnet synchronous motors, rated at 13 kW power at 7200 RPM operating speed. The motor axial length is approximately 2.0 inches, and its outer diameter is approximately 5.5 inches, yielding a tip speed of about 53 m/sec.

The intention of the effort described here is to build a motor for this type of application; however, only analytical results are given in this paper.

III. Approach

The basic configuration considered here consists of a double-Halbach array of permanent magnets arranged on both sides of the copper windings. The windings comprise the stator, and the magnet arrays comprise a double-rotor. Figure 1 shows the magnets and windings of a ten-pole-pair configuration as modeled in Maxwell 3D electromagnetic finite element analysis software. Since a full 3D analysis is time-consuming, a quicker estimation of motor power and losses was devised using a two-dimensional analysis based on equations for magnetic flux within a double-Halbach array.
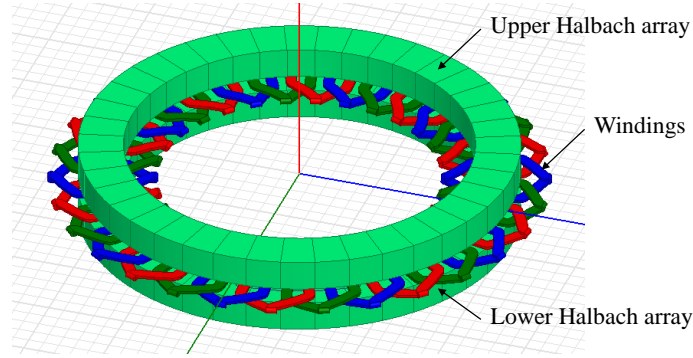
Figure 1. Ten-pole-pair double-Halbach array axial flux motor configuration.

First, a simple two-dimensional magnetostatic analysis was done to look at the effect of various parameters on the flux within the air gap, which is proportional to the motor torque. This analysis was performed on a single pole-pair motor segment, as shown in Figure 2. The magnet array is modeled in rectangular coordinates, as if the motor of figure 1 were unwrapped circumferentially (mean radius model). Here the circumferential direction is along the *x*-axis, the axial direction is along the *y*-axis, and the radial direction is along the *z*-axis.

The static magnetic force on the conductors is calculated assuming the flux density produced by the double-Halbach array, which is then used to estimate the motor torque and power. The torque density and power density are then calculated from the component masses. Efficiency is estimated by determining the resistive and eddy current losses in the conductors. All equations were solved using Mathematica software, and then results were validated with Maxwell 2D and 3D finite element analysis.
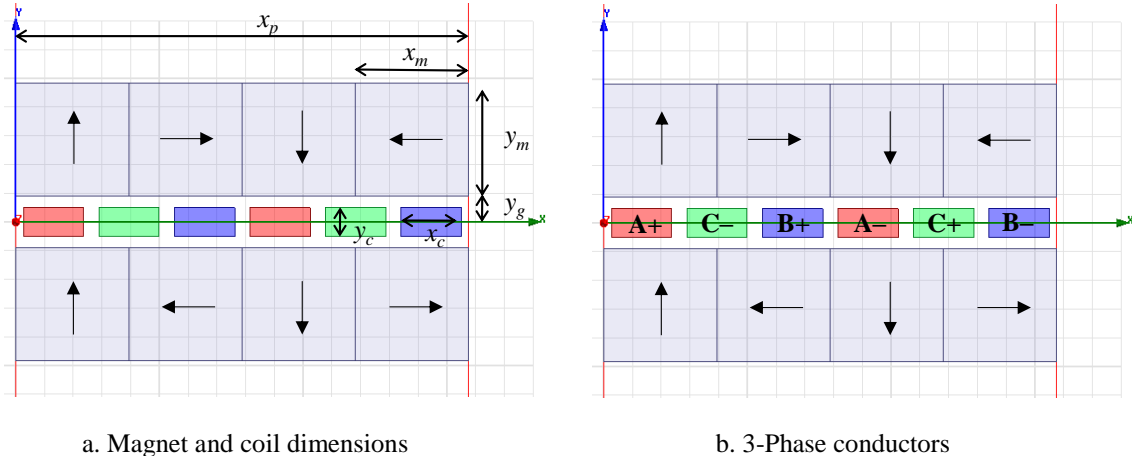
a. Magnet and coil dimensions   b. 3-Phase conductors
Figure 2. Single pole pair for magnetostatic analysis with conductors in a single row and $\epsilon=1$.

IV. Analysis

Figure 2a shows the dimensions of a pole pair of the unwrapped motor. The motor being modeled has an outer radius of r_o and a radial thickness of Δr. The average radius of the motor is $r_a = r_o - \frac{1}{2}\Delta r$. The circumferential

American Institute of Aeronautics and Astronautics

distance between like poles, x_p, is merely the average circumference of the motor divided by the number of pole pairs p, or $x_p = 2\pi r_a/p$. The magnet circumferential length is $x_m = \epsilon\, x_p/n_m$, where n_m is the number of magnets in each pole pair (shown as equal to four in figure 2) and ϵ is the magnet embrace (shown as equal to one in figure 2). The magnet axial length is y_m, and the magnet radial length z_m is set equal to the rotor radial thickness, or $z_m = \Delta r$. The gap between the magnet arrays is equal to $2y_g$. For the conductors, each phase side has a circumferential length of x_c, an axial length of y_c, and a radial length equal to the rotor radial length, or $z_c = \Delta r$.

The magnetic flux between a rectangular double Halbach array is given by[11]

$$B_x = 2B_R e^{-ky_g}(1 - e^{-ky_m})\frac{\sin(\epsilon\pi/n_m)}{\pi/n_m}\sin kx \sinh ky \tag{1}$$

and

$$B_y = 2B_R e^{-ky_g}(1 - e^{-ky_m})\frac{\sin(\epsilon\pi/n_m)}{\pi/n_m}\cos kx \cosh ky, \tag{2}$$

where $k = 2\pi/x_p$. Clearly equations 1 and 2 show only the fundamental component of the flux density; the harmonics are ignored. However, the force calculation is quite accurate using only these equations.

It is assumed that there is a three-phase excitation in the windings, as shown in figure 2b. The currents are in the z-direction, and are given by

$$\begin{aligned} I_A &= I_{pk}\cos(p\omega_r t + \phi) \\ I_B &= I_{pk}\cos\left(p\omega_r t + \phi - \tfrac{2\pi}{3}\right) \\ I_C &= I_{pk}\cos\left(p\omega_r t + \phi - \tfrac{4\pi}{3}\right), \end{aligned} \tag{3}$$

where I_{pk} is the peak current in the winding in Ampere-turns, ω_r is the rotor speed in rad/s, and ϕ is an arbitrary phase shift. The windings are distributed between the magnet arrays, one example of which is shown in figure 2b. There the windings are aligned in one row, but they can be distributed in any configuration, especially considering the reality of winding placement. The force calculation will be magnetostatic, so an arbitrary time is chosen to perform the calculations.

The magnetostatic force on a piece of conductor is given by $dF = IL \times dB$. So for a given winding configuration, the torque-producing force on a single phase side coil segment within a double-Halbach array can be directly calculated using equations 2 and 3:

$$F_c = J\Delta r \int_{x_1}^{x_2}\int_{y_1}^{y_2} B_y\, dxdy, \tag{4}$$

where J is the current density within the coil segment. If the phase side coil segment has dimensions of $x_c = x_2 - x_1$ in the circumferential direction, and $y_c = y_2 - y_1$ in the axial direction, then $J = I/(x_c y_c)$. Assuming that J is constant across the conductor cross section, then the force on a phase side coil segment in the x-direction is

$$F_c = [2JB_R\Delta r]\left[\frac{e^{-ky_g}(1-e^{-ky_m})}{k^2}\right]\left[\frac{\sin(\epsilon\pi/n_m)}{\pi/n_m}\right]\sin kx|_{x_1}^{x_2}\sinh ky|_{y_1}^{y_2}. \tag{5}$$

The total force within a pole pair is just the sum of the forces due to all the conductors within that pole pair. Assuming the three phases are acting within each pole pair, and each phase has two coil phase sides (plus and minus), then the pole pair force is

$$F_p = \sum_{c=1}^{6} F_c, \tag{6}$$

The motor torque can be calculated by multiplying the force per pole pair by the average radial distance to the center of rotation, r_a, and the number of pole pairs:

$$T = pr_a F_p, \tag{7}$$

and the motor power is then the torque multiplied by the rotor speed ω_r:

$$P = T\,\omega_r = T\ RPM\ \pi/30. \tag{8}$$

4

The mass used to calculate torque density and power density includes only the conductors and magnets. The magnet mass is given by

$$m_m = 2p\rho_m \epsilon x_p y_m \Delta r \, , \tag{9}$$

where ρ_m is the magnet mass density. The conductor mass is calculated assuming circular end turns for simplicity, and is given by

$$m_c = 6p\eta\rho_c x_c y_c (\Delta r + \pi r_c), \tag{10}$$

where η is the packing factor of conductor within the coil area, ρ_c is the conductor mass density, and r_c is half the distance between the turns of the coil, as shown in Figure 3. For the configuration in Figure 2a, $r_c = x_p/4$.
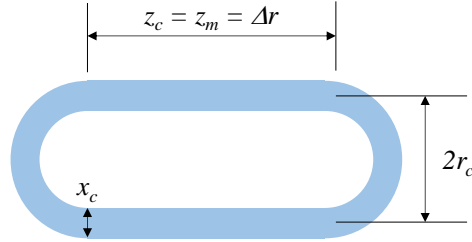
Figure 3. Coil dimensions.

Next we consider the losses within the motor. It is expected that the dominant loss in this design will be the I^2R loss in the conductors. The total conductor resistive loss is

$$P_c = 6p J_{rms}^2 x_c y_c (\Delta r + \pi r_c)/(\sigma\eta), \tag{11}$$

where σ is the conductivity of the conductor material, and J_{rms} is the rms value of the current density J based on the Ampere-turns I_{pk} in equation 3.

Eddy current loss in the conductors can be estimated using from the fundamental component of the time-varying magnetic flux. The eddy current loss for round conductors is[4]

$$P_e = \frac{\pi^2}{4}\sigma f^2 d^2 V_c \left[\left(B_x^2 + B_y^2 \right)_{pk}^2 + B_{zpk}^2 \right], \tag{12}$$

where f is the electrical frequency in Hz, d is the conductor strand diameter, V_c is the volume of the conductors without end turns, and B_{zpk} is the peak flux density along the conductor length. The electrical frequency is simply the product of the rotor speed and the number of pole pairs, or $f = p\, RPM/60$.

Other losses in the motor include eddy current losses in the magnets, windage losses, and bearing losses. Eddy current losses in the magnets should be very low, since the time-varying field in the magnets due to the conductors is very low. A discussion of eddy current loss in permanent magnets can be found in Ding and Mi.[12] Equations for windage and bearing losses can be found in Gieras.[4]

V. Discussion

Observing the equations for force, torque, and mass can tell us much about the importance of various parameters. In order to maximize torque, the conductor force given by equation 5 must be maximized. From the expression in the first pair of brackets in equation 5, we see that the force is directly proportional to current density, PM remanence flux, and radial length. Observing the expression in the second pair of brackets of equation 5, we can see that minimizing ky_g, which is proportional to the ratio of air gap to magnet circumferential length, will maximize F_x. Similarly maximizing ky_m, which is proportional to the ratio of the magnet axial thickness to the magnet

circumferential length (magnet aspect ratio), will maximize F_x. Finally, observing the term $\sin(\epsilon\pi/n_m)/(\pi/n_m)$, we can see that increasing n_m and increasing ϵ will maximize F_x (Figure 4). However, the goal is not just to maximize the torque, but to maximize the torque density. So increasing the magnet thickness for example would increase flux density, but also increase the mass.
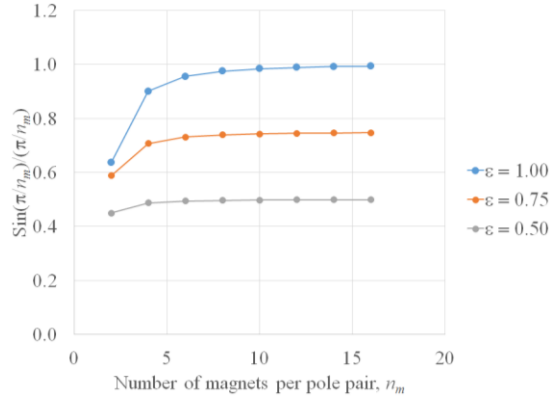
Figure 4. Effect of number of magnets per pole pair.

The power density is proportional to the torque density, which is (not considering end turns or non-active materials)

$$\frac{T}{m} \cong \frac{F_p r_a}{\Delta r\left(6\rho_c \eta x_c y_c + 2\rho_m \epsilon x_p y_m\right)}. \tag{13}$$

Substituting equation 5 into equation 13, we see that the torque density is proportional to

$$\frac{T}{m} \propto [J B_R r_a]\left[\frac{e^{-ky_g}\left(1-e^{-ky_m}\right)}{k^2\left(3\rho_c x_c y_c + \rho_m \epsilon x_p y_m\right)}\right]\left[\frac{\sin(\epsilon\pi/n_m)}{\pi/n_m}\right]. \tag{14}$$

From the expression in the first pair of brackets in equation 14, we see that the torque density is proportional to the average radius, and the radial thickness has cancelled out (as compared to equation 5 for torque). For torque density, note that the coil dimensions are counted twice – once implicitly in current density and once explicitly in coil mass. Packing a maximum amount of current into a small area benefits the torque density; however, the current density and coil dimensions will end up being constrained by temperature rise within the conductor. Looking at the expression in the second pair of brackets, considering only magnet mass in the denominator, and simplifying, we can see the torque density based on magnet mass alone is proportional to

$$\frac{T}{m_m} \propto \frac{e^{-ky_g}\left(1-e^{-ky_m}\right)}{ky_m}. \tag{15}$$

Equation 15 shows that even though the torque increases with increasing ky_m, the torque density actually maximizes at $ky_m \rightarrow 0$.

The power density is the torque density multiplied by the rotor speed. Clearly the power density increases with increasing rotor speed; however, the rotor tip speed will be limited by structural considerations. There will need to be a support structure, such as a containment ring, holding the magnets in the rotor. Depending on the materials used, the strength and mass of this containment ring will affect the power density through allowable tip speed and ring mass. This is why the high strength and low density of carbon fiber composite containment rings are considered for these configurations.

VI.   Results

The equation for the conductor force was used in Mathematica software to calculate the total force in the motor for the single row winding configuration. Then the torque, power, and resistive loss were calculated as functions of various parameters. The results were verified by running some of the cases in a Maxwell 2D magnetostatic analysis. Generally the force results were good to within 1% error as compared to Maxwell 2D.

6

The coil fill factor was assumed to be 50%, and the current density ranged from 3-30 A/mm², to cover the range of cooling from natural convection to liquid cooling. It was assumed that some form of cooling is added to maintain an average conductor temperature at 120ºC for loss calculation purposes. The mass of the cooling system is not included in the power density calculation. For all calculations, a fixed outer diameter of 139.7 mm (5.5 in) was used. The baseline rotor speed is assumed to be 7200 RPM (53 m/s tip speed), but rotor speeds of 14,400 RPM (tip speed = 106 m/s) and 28,800 RPM (212 m/s) were also used, and the additional mass of a gearbox was added into the power density calculation. At 7200 RPM, a torque of 17.3 N-m is required to give 13 kW.

First, the effect of motor inner diameter and current density on power, power density, and efficiency was investigated for 16 pole pairs, a coil thickness of 3 mm, and a ratio of magnet axial thickness to circumferential thickness of one. A value of 16 pole pairs was chosen because it yields an electrical frequency of 1920 Hz, which is at the upper end of the desirable range. Figures 5-7 show that the ratio of motor inner to outer diameter has a maximum power density near 0.7 and minimum resistive loss near 0.5. However, the power is higher for a smaller inner diameter. The current density increases power and power density at the expense of efficiency, as expected. To obtain the required motor power of 13 kW with less than 1% resistive loss requires a current density of about 20 A/mm² and ID/OD ratio of 0.6, so this is used in further calculations. This yields a power density of nearly 13 kW/kg, based on copper and magnet mass alone. Figure 8 shows the importance of the conductor strand diameter for eddy current loss for $J = 20$ A/mm².
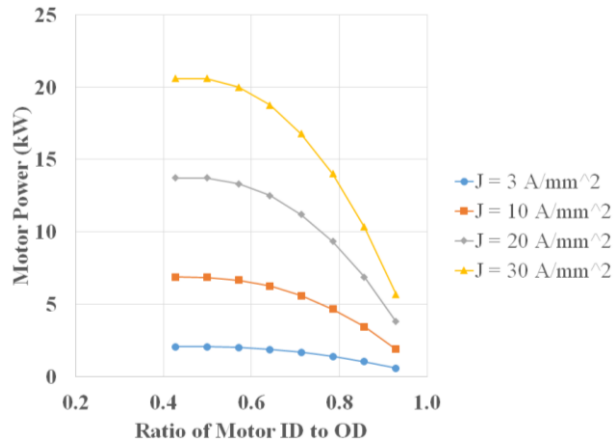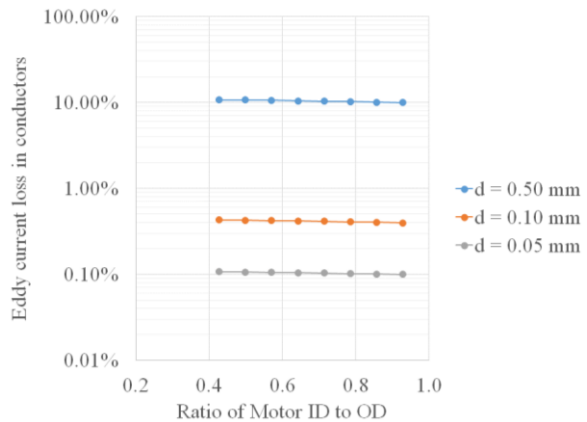

Figure 5. Power vs. ID/OD.
16 pole pairs, $y_c = 3$ mm,
magnet aspect ratio = 1.0
7200 RPM
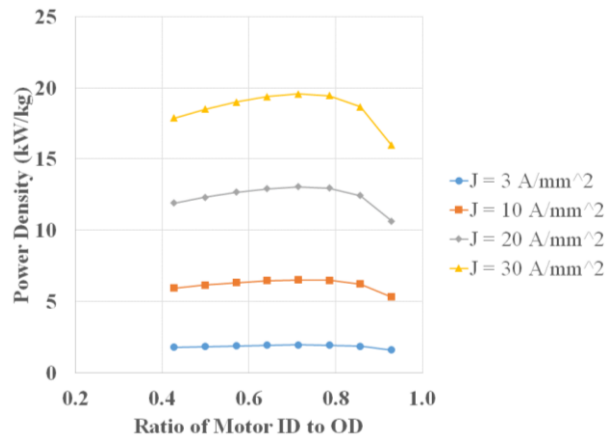
Figure 6. Power density vs. ID/OD.
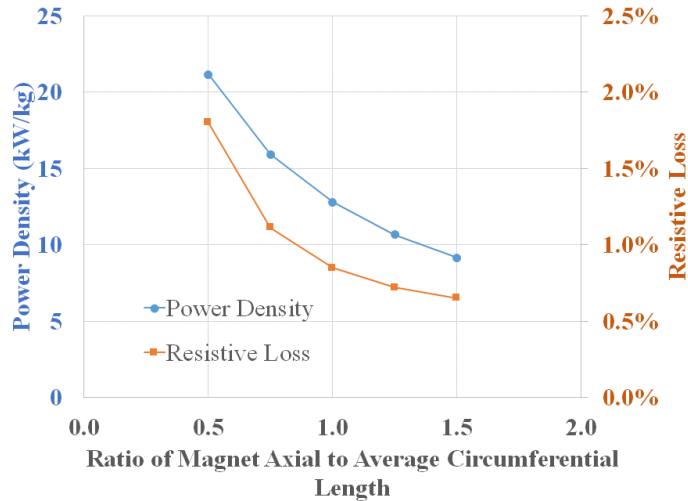16 pole pairs, $y_c = 3$ mm,
magnet aspect ratio = 1.0,
7200 RPM
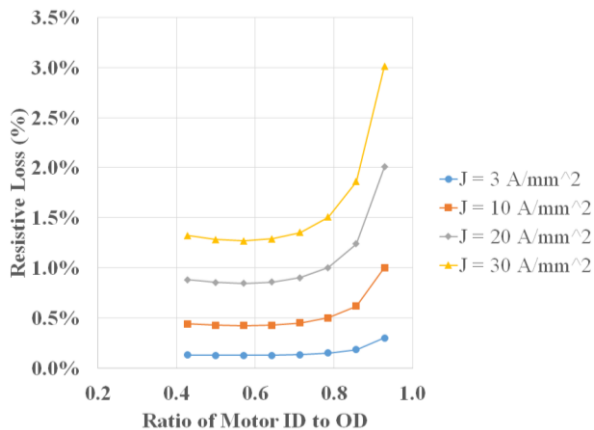
Figure 7. Resistive loss vs. ID/OD.
16 pole pairs, $y_c = 3$ mm,
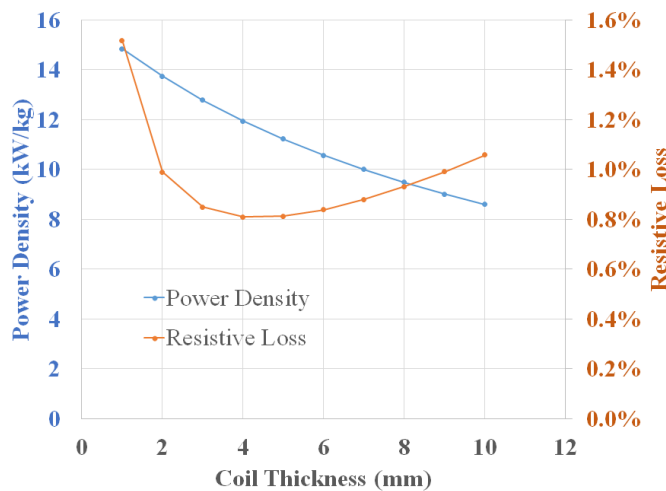magnet aspect ratio = 1.0, 7200 RPM

Figure 8. Conductor eddy loss vs. ID/OD.
16 pole pairs, $y_c = 3$ mm, $J = 20$ A/mm²
magnet aspect ratio = 1.0, 7200 RPM

7
American Institute of Aeronautics and Astronautics

Next, the effect of magnet axial thickness was studied. Figure 9 shows how the magnet aspect ratio affects power density and resistive loss for a power of 13 kW, 16 pole pairs, and coil axial thickness of 3 mm. In the discussion, we determined that decreasing the magnet aspect ratio maximizes power density, which can be seen in Figure 9. However, the current density required to reach the required power of 13 kW increases with decreasing aspect ratio, which causes the resistive loss to increase. Again, requirements for power density and efficiency are at odds, and an aspect ratio of around 1.0 yields a resistive loss of less than 1%, so that value is used in further calculations.

Figure 9. Effect of magnet aspect ratio on power density and efficiency.
16 pole pairs, y_c = 3 mm, rotor ID/OD = 0.6,
current density varied to give 13 kW power at 7200 RPM

Next the effect of the coil axial thickness was studied. Figure 10 shows the power density and resistive loss as a function of coil axial thickness, for 13 kW, 16 pole pairs, magnet aspect ratio of 1.0, and ratio of rotor ID to OD of 0.6. As expected, the power density increases with decreasing coil thickness, because a smaller coil thickness yields a smaller air gap between the magnet arrays. The resistive loss at low coil thickness is higher because a higher current density is required to reach 13 kW because of the smaller coil size. The resistive loss at high coil thickness is higher because of the lower magnetic field resulting from a larger gap between magnet arrays. A coil thickness of 3 mm was chosen as the optimal value for further calculations.


Figure 10. Effect of coil thickness on power density and efficiency.
16 pole pairs, rotor ID/OD = 0.6, magnet aspect ratio = 1.0,
current density varied to give 13 kW power at 7200 RPM

American Institute of Aeronautics and Astronautics

Finally, the effect of the number of pole pairs was studied. In this case, the magnet thickness was set to be constant over the pole count range resulting in a maximum magnetic flux density of 1.0 T in the gap between magnets. Figure 11 shows that increasing the number of pole pairs increases power density. The magnet mass remains the same over the pole count range; however, the higher pole count reduces the coil end turn mass, increasing power density. As pole count increases, the coil cross sectional area decreases as well as the turn length, which are competing factors with regard to resistance. The higher pole count also increases the number of coils, also increasing resistance. The combination of these factors results in an optimum pole pair count of 16 for minimizing resistive loss.

The higher pole count also increases the electrical frequency, which affects the eddy current loss in the conductor and in the magnets, as well as switching losses in the power electronics. Again, the baseline pole pair number of 16 was chosen to keep the electrical frequency below 2000 Hz.
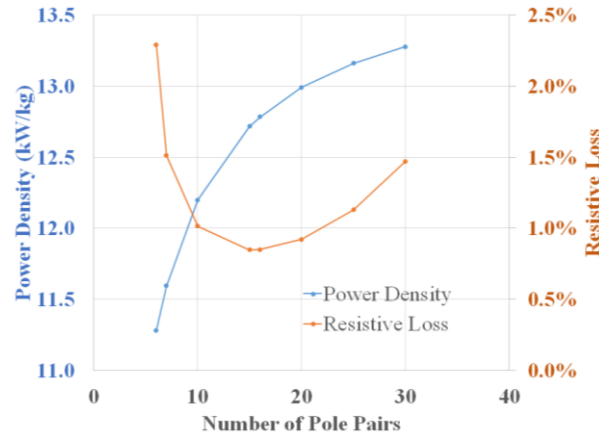
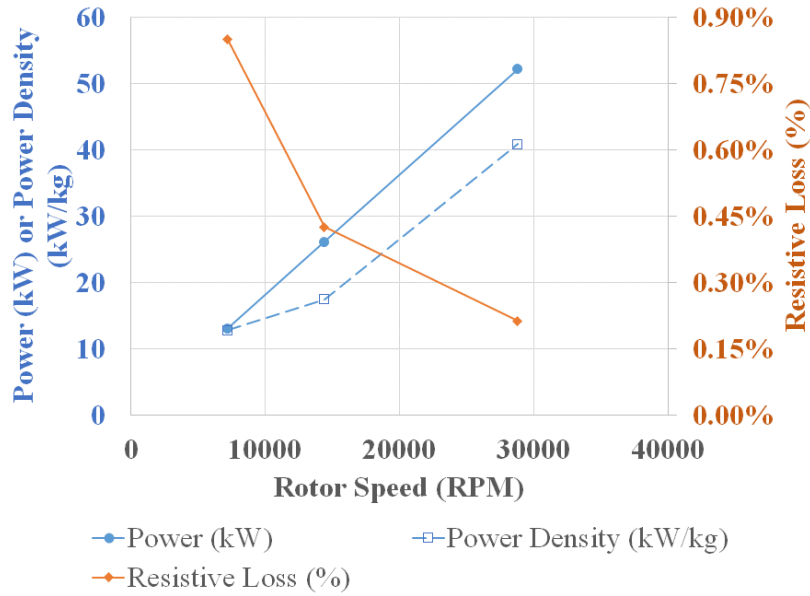**Figure 11. Effect of pole pairs on power density and resistive loss.**
y_c = 3 mm, rotor ID/OD = 0.6, y_m = 5.49 mm,
current density varied to give 13 kW power at 7200 RPM

The tip speed of the rotor at 7200 RPM is only 53 m/sec, which is relatively low. A higher speed should improve the motor's performance if it remains a direct-drive motor, but in this case it will require a gearbox to produce the correct speed for the fan. Based on gearbox technology from the year 2000, Brown et al.[13] gave an expression for the weight of a gearbox as

$$W = 94 HP^{0.76} \frac{RPM_r^{0.13}}{RPM_f^{0.89}}, \tag{16}$$

where W is the gearbox weight in lbs, HP is the motor power in horsepower (13 kW is approximately 17 HP), and RPM_r is the motor rotor speed and RPM_f is the fan speed, both in revolutions per minute.

If we simply increase the speed of the optimal 7200 RPM motor, we see that power, power density, and efficiency are all increased, even with the added gearbox weight, as shown in Figure 12. However, if the higher speed motors are re-sized to the 13 kW target, it becomes clear that adding a gearbox negatively impacts the motor performance for both power density and resistive loss, as shown in Table 1.

American Institute of Aeronautics and Astronautics

Figure 12. Effect of running the motor at higher speed.

Rotor Speed (RPM)	Drive Type	Rotor ID/OD	Pole Pairs	Magnet Aspect Ratio	Coil Thickness (mm)	Current Density (A/mm^2)	Power Density (kW/kg)	Resistive Loss
7200	Direct	0.50	16	1.0	3.0	20.0	12.8	0.85%
14,400	Gearbox	0.71	8	0.375	2.0	21.3	11.2	0.87%
28,800	Gearbox	0.71	4	0.25	1.0	24.8	12.1	0.97%

Table 1. Motor parameters for 13 kW power vs. rotor speed.

   The 7200 RPM optimal motor shown in Table 1 was modeled in Maxwell 3D to obtain transient results for torque, magnet eddy current losses, and resistive losses. The coils were modeled as forming two rows within the air gap. To reduce computational time, one pole pair was included in the analysis, with a single Halbach magnet array and a symmetric boundary condition running through the center of the gap, as shown in Figure 13. A slotless configuration was difficult to model in Maxwell; therefore, a slotted configuration was modeled, with the stator core assumed to be vacuum. This caused the coils to be much more compact than in the optimal design, increasing the current density, and therefore the resistive loss. However, a comparison of results for both the simple analysis and the Maxwell 3D magnetostatic and transient analysis could be easily performed, and results are shown in Table 2. The simple analysis underestimated the torque by about 4%, and the resistive loss by about 6% compared to the Maxwell 3D prediction.

American Institute of Aeronautics and Astronautics
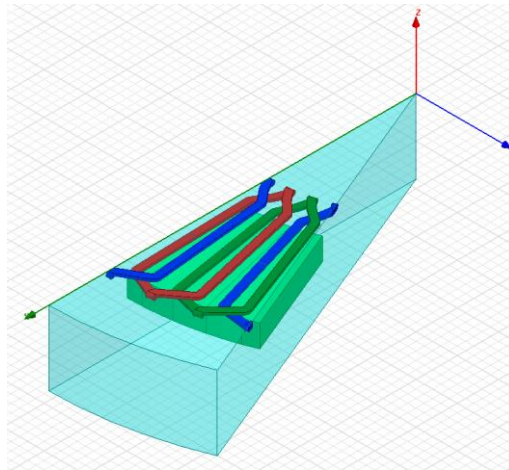
Figure 13. Maxwell 3D motor model.

Analysis	Torque (N-m)	Resistive Loss (%)	Eddy Current Loss in 0.1mm-diameter Conductors (%)	Eddy Current Loss in Magnets (%)
Equation-based magnetostatic – large coils (optimal design)	17.3	0.85%	0.11%	-
Equation-based magnetostatic – compact coils/high J	16.3	7.6%	0.06%	-
Maxwell 3D magnetostatic – compact coils/high J	16.6	-	-	-
Maxwell 3D transient – compact coils/high J	16.9	8.1%	-	0.02%

Table 2. Comparison of analysis results.

VII. Conclusions

With target values for power density of 13 kW/kg and resistive loss of 1%, this study showed the difficulty of achieving this goal within the constraints of the fan speed, geometry, and electrical frequency. A direct-drive 7200 RPM motor was designed that achieved 12.8 kW/kg (including only magnet and copper weight), 0.85% resistive loss, and a 0.1% eddy current loss with 0.05 mm diameter conductors. The added mass of the structure and cooling system still need to be included, which should reduce power density by a significant amount. In addition, other losses such as bearing loss and windage loss should be included in the efficiency calculation, as well as higher order effects. Future plans include investigating other motor types and configurations with the same goal of reducing losses to 1% while maximizing power density.

References

[1]Bradley, Marty K. and Droney, Christopher K., "Subsonic Ultra Green Aircraft Research: Phase I Final Report," NASA/CR-2011-216847, 2011.

[2]Brown, Gerald V., "Efficient Flight-Weight Electric Systems," *NASA Fundamental Aeronautics Program 2012 Technical Conference*, Cleveland, OH, 2012.

[3]Jansen, Ralph H., Brown, Gerald V., Felder, James L., and Duffy, Kirsten P., "Turboelectric Aircraft Drive Key Performance Parameters and Functional Requirements," *51st AIAA/SAE/ASEE Joint Propulsion Conference*, AIAA-2015-3890, Orlando, FL, 2015.

[4]Gieras, J. F., Wang, R. J., and Kamper, M. J., *Axial Flux Permanent Magnet Brushless Machines*, Springer, 2008.

American Institute of Aeronautics and Astronautics

[5]Capponi, F. G., De Donato, G., and Caricchi, F., "Recent Advances in Axial-Flux Permanent-Magnet Machine Technology," *IEEE Transactions on Industry Applications*, vol. 48, no. 6, pp. 2190-2205.

[6]Virtič, Peter, Pišek, Peter, Marčič, Tine, Hadžiselimovič, Miralem, and Štumberger, Bojan, "Analytical Analysis of Magnetic Field and Back Electromotive Force Calculation of an Axial-Flux Permanent Magnet Synchronous Generator with Coreless Stator," *IEEE Transactions on Magnetics*, vol. 44, no. 11, November 2008.

[7]Huang, S., Luo, J., Leonardi, F., and Lipo, T. A., "A Comparison of Power Density for Axial Flux Machines Based on General Purpose Sizing Equations," *IEEE Transactions on Energy Conversion*, vol. 14, no. 2, pp. 185-192, 1992.

[8]Mahmoudi, A., Rahim, N. A., and Ping, H. W., "Axial-Flux Permanent-Magnet Motor Design for Electric Vehicle Direct Drive Using Sizing Equation and Finite Element Analysis," *Progress in Electromagnetics Research*, vol. 122, pp. 467-496, 2012.

[9]Bumby, J. R., Martin, R., Mueller, M. A., Spooner, E., Brown, N. L., and Chalmers, B. J. "Electromagnetic Design of Axial-Flux Permanent Magnet Machines," *IEEE Proceedings – Electric Power Applications*, vol. 151, no. 2, March 2004.

[10]Merlin, Peter, "LEAPTech to Demonstrate Electric Propulsion Technologies," *NASA Armstrong Features*, NASA, 16 March 2015. Web. Accessed 17 May 2016. < https://www.nasa.gov/centers/armstrong/features/leaptech.html >.

[11]Halbach, Klaus, "Application of Permanent Magnets in Accelerators and Electron Storage Rings," *Journal of Applied Physics*, vol. 57, 3605, 1985.

[12]Ding, Xiaofeng and Mi, Chris, "Modeling of Eddy Current Loss in the Magnets of Permanent Magnet Machines for Hybrid and Electric Vehicle Traction Applications," *Proceedings of the 2009 IEEE Vehicle Power and Propulsion Conference*, pp. 419-424, 2009.

[13]Brown, G. V., Kascak, A. F., Ebihara, B., Johnson, D., Choi, B., Siebert, M. and Buccieri, C., "NASA Glenn Research Center Program in High Power Density Motors for Aeropropulsion," NASA/TM-2005-213800, 2005.

American Institute of Aeronautics and Astronautics